

Article

# Bismuth-Based Oxyborate Piezoelectric Crystals: Growth and Electro-Elastic Properties

Feifei Chen <sup>1</sup>, Xiufeng Cheng <sup>1</sup>, Fapeng Yu <sup>1,\*</sup>, Chunlei Wang <sup>2</sup> and Xian Zhao <sup>1</sup>

<sup>1</sup> State Key Laboratory of Crystal Materials, Advanced Research Center for Optics, Shandong University, Jinan 250100, China; ffchen2013@126.com (F.C.); xfcheng@sdu.edu.cn (X.C.); xianzhao@sdu.edu.cn (X.Z.)

<sup>2</sup> School of Physics, Shandong University, Jinan 250100, China; wangcl@sdu.edu.cn

\* Correspondence: fapengyu@sdu.edu.cn

Received: 13 December 2018; Accepted: 2 January 2019; Published: 6 January 2019



**Abstract:** The non-centrosymmetric bismuth-based oxyborate crystals have been extensively studied for non-linear optical, opto-electric and piezoelectric applications. In this work, single crystal growth and electro-elastic properties of  $\alpha$ -BiB<sub>3</sub>O<sub>6</sub> ( $\alpha$ -BIBO) and Bi<sub>2</sub>ZnB<sub>2</sub>O<sub>7</sub> (BZBO) crystals are reported. Centimeter-sized  $\alpha$ -BIBO and BZBO crystals were grown by using the Kyropoulos method. High resolution X-ray diffraction tests were performed to assess the crystal quality. The full-width at half-maximum values (FWHM) of the rocking curves were evaluated to be 35.35 arcsec and 47.85 arcsec for  $\alpha$ -BIBO and BZBO samples, respectively. Moreover, the electro-elastic properties of  $\alpha$ -BIBO and BZBO crystals are discussed and summarized, based on which the radial extensional and the face shear vibration modes were studied for potential acoustic device applications. The radial extensional mode electro-mechanical coupling factors  $k_p$  were evaluated and found to be 32.0% and 5.5% for  $\alpha$ -BIBO and BZBO crystals, respectively. The optimal crystal cuts with face shear mode were designed and found to be (YZt)/−53° (or (YZt)/37° cut) for  $\alpha$ -BIBO crystal, and (ZXt)/±45° cut for BZBO crystal, with the largest effective piezoelectric coefficients being in the order of 14.8 pC/N and 8.9 pC/N, respectively.

**Keywords:**  $\alpha$ -BiB<sub>3</sub>O<sub>6</sub>; Bi<sub>2</sub>ZnB<sub>2</sub>O<sub>7</sub>; single crystal growth; electro-elastic properties

## 1. Introduction

Oxyborate crystals are important multi-functional crystal materials with comprehensive performances in non-linear optical (NLO), laser, and piezoelectric fields [1–6]. In recent years, the oxyborate crystals, especially the bismuth-based oxyborate crystals, have been paid a great deal of attention for exploring and designing new optical and piezoelectric devices, due to the abundant B-O groups and the bismuth lone pair structure [7,8].

The bismuth-based oxyborate compounds were first discovered in 1962 from the Bi<sub>2</sub>O<sub>3</sub>-B<sub>2</sub>O<sub>3</sub> binary phase diagram, where the Bi<sub>24</sub>B<sub>2</sub>O<sub>39</sub>, Bi<sub>4</sub>B<sub>2</sub>O<sub>9</sub>, Bi<sub>3</sub>B<sub>5</sub>O<sub>12</sub>, BiB<sub>3</sub>O<sub>6</sub>, and Bi<sub>2</sub>B<sub>8</sub>O<sub>15</sub> crystals were discovered and confirmed [9–13]. Among these compounds, the monoclinic  $\alpha$ -BiB<sub>3</sub>O<sub>6</sub> ( $\alpha$ -BIBO) crystal was reported to be a valuable NLO material, showing an excellent second harmonic generation (SHG) effect, comparable to the commercialized KTiOPO<sub>4</sub> (KTP) crystal [13,14]. Furthermore, active studies were performed for new NLO crystal materials in the ternary Bi<sub>2</sub>O<sub>3</sub>-MO-B<sub>2</sub>O<sub>3</sub> system (MO is metal oxide), and a new non-centrosymmetric crystal Bi<sub>2</sub>ZnB<sub>2</sub>O<sub>7</sub> (BZBO) with orthorhombic symmetry was obtained [15,16]. To date, the  $\alpha$ -BIBO and BZBO crystals have been successfully grown in labs, and their NLO and piezoelectric properties have been discussed [17–21]. However, there remains problems during the single crystal growth, and critical growth parameters have not been optimized yet, especially for the  $\alpha$ -BIBO crystal. The electro-elastic properties and the piezoelectric vibration modes of the  $\alpha$ -BIBO and BZBO crystals are worth studying further. For example, the radial extensional and

face shear vibration modes are useful for exploring new acoustic wave devices based on the lamb waves and guided waves [22–24].

In this paper, the monoclinic  $\alpha$ -BIBO and orthorhombic BZBO crystals grown by using the Kyropoulos method with modified thermal profiles, are studied. The electro-elastic properties, including the dielectric, elastic, electromechanical and piezoelectric properties of the  $\alpha$ -BIBO and BZBO crystals were compared comprehensively, taking advantage of the impedance method. The radial extensional and face shear vibration modes for  $\alpha$ -BIBO and BZBO crystals were evaluated for potential acoustic wave device applications.

## 2. Experimental Section

### 2.1. Single Crystal Growth

The  $\alpha$ -BIBO and BZBO crystals are all congruent compounds and can be grown by using the Kyropoulos method. Firstly, polycrystalline  $\alpha$ -BIBO and BZBO powders were synthesized by traditional solid-state reaction technique. The raw materials were weighted according to their stoichiometric ratio (molar ratio of  $\text{Bi}_2\text{O}_3$ :  $\text{H}_3\text{BO}_3$  = 1:6 for  $\alpha$ -BIBO and  $\text{Bi}_2\text{O}_3$ : $\text{ZnO}$ : $\text{H}_3\text{BO}_3$  = 1:1:2 for BZBO crystals). To prepare the polycrystalline  $\alpha$ -BIBO powders, 1.0 mol%  $\text{H}_3\text{BO}_3$  in excess was added to the raw materials in order to compensate for the evaporation of the  $\text{B}_2\text{O}_3$  during the solid-state reaction and crystal growth processes, which was proved to be in favor of growing high quality  $\alpha$ -BIBO single crystals. Secondly, the raw materials were ground and dry mixed thoroughly for more than 12 h (YGJ-5KG, no use of ball milling), then they were pressed into column blocks. The blocks were sintered at 400 °C for more than 4 h in order to decompose the  $\text{H}_3\text{BO}_3$  completely, then charged into a platinum (Pt) crucible ( $\varphi$  = 10 cm, H = 12 cm). The crucible was 70% fulfilled with the sintered polycrystalline blocks and loaded into a programmable controlled furnace, which was progressively heated up to 800 °C above the melting points of the  $\alpha$ -BIBO and BZBO compounds. Thirdly, the melts were homogenized with a Pt stirrer for more than 24 h, and then kept for 48 h to ensure the uniformity of the melt in the crucible. Fourthly, the temperature was then slowly decreased down to an appropriate temperature for the seeding and crystal growth process.

The principal component of the crystal growth equipment is a tube furnace with electric stove wire as the heating source. The furnace is designed with a special and stable temperature gradient along the axial direction. The schematic diagram of the crystal growth equipment is shown in Figure 1a. It is known that the thermal profile is crucial for crystal growth. Prior to the single crystal growth, the thermal gradient should be determined. In this work, for evaluation of the thermal gradient, the temperature was measured from the bottom of the crucible to the top, and then from the top back to the bottom. To ensure the accuracy of the measurement, the temperature gradients were measured at different temperature points and for each measurement, the dwelling time was kept for 10–15 min. Figure 1b,c present the optimized temperature gradient distributions in the furnace for  $\alpha$ -BIBO and BZBO crystals, respectively.

According to our experiments, we found that the axial temperature gradient is sensitive to the growth of BZBO and  $\alpha$ -BIBO crystals, since the growth temperature range of these crystals is quite narrow ( $\sim 4$  °C). A narrow axial temperature gradient of  $< 2$  °C/cm in the modified thermal profile is beneficial for growing BZBO and  $\alpha$ -BIBO crystals stably, thereby improving the crystal quality. In this study, the desired temperature gradients were controlled to be  $< 1$  °C/cm and  $< 2$  °C/cm approach to the surface of the  $\alpha$ -BIBO and BZBO melts, respectively. To avoid the emergence of poly-crystals, a very low cooling rate (0.1–0.5 °C/day) was adapted during the crystal growth.

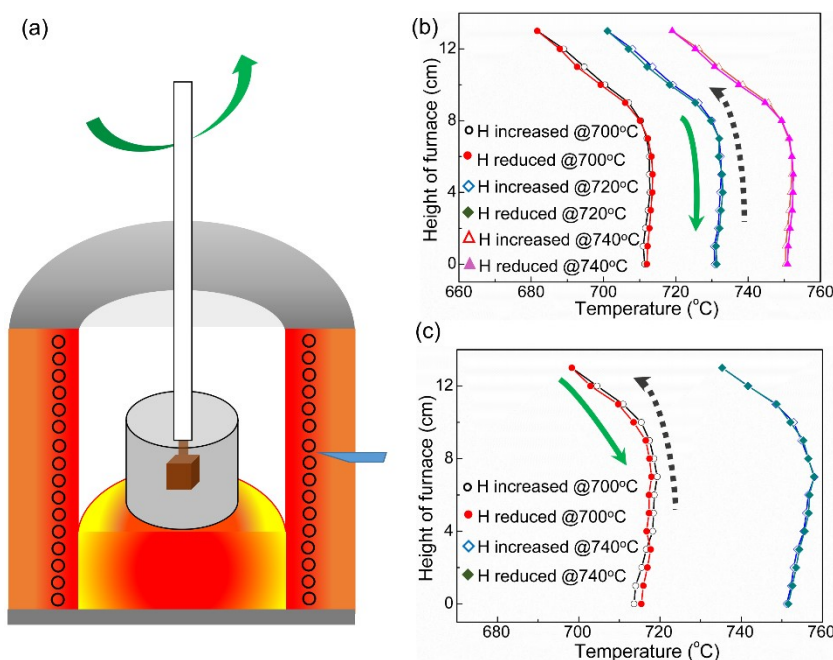


**Figure 1.** The schematic diagram of the crystal growth furnace (a) and the temperature gradient in the furnace used for  $\alpha$ - $\text{BiB}_3\text{O}_6$  ( $\alpha$ -BIBO) (b) and  $\text{Bi}_2\text{ZnB}_2\text{O}_7$  (BZBO) (c) crystals.

During the crystal growth process, a bi-directional rotation was adopted to improve the homogeneity of the melt. However, due to the high viscosity, the viscous forces induced by the melt would increase with increasing crystal dimension, which would damage the neck between the crystal seed and bulk crystal [12]. Thus, an appropriate rotation rate should be applied. During the growth of  $\alpha$ -BIBO and BZBO crystals, a medium rotation rate of 10–15 rpm was adapted and controlled. The crystal growth period was selected to be 2 to 8 weeks. When the crystal reached the expected dimension, it was pulled out of the melt slowly and hung over the melt for 1–2 h, then cooled down to room temperature with a low rate of 5–20 °C. Figure 2 presents the as-grown  $\alpha$ -BIBO and BZBO crystals with distinguished habitual facets. Though some impurities (polycrystalline raw materials) adhered on the surface, the total crystals were transparent inside. The impurities were generated when pulling the crystal out of the melt.

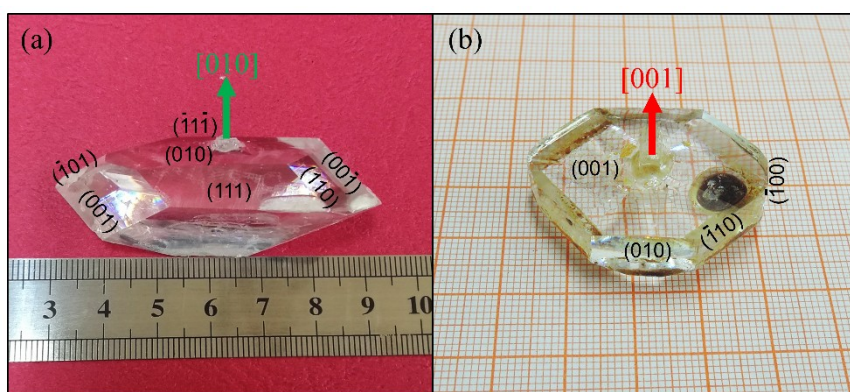


**Figure 2.** The as-grown  $\alpha$ -BIBO (a) and BZBO (b) single crystals.

## 2.2. High-Resolution X-Ray Diffraction

The qualities of the grown  $\alpha$ -BIBO and BZBO crystals can be evaluated by using the high-resolution X-ray diffraction (HRXRD) method. In our study, the HRXRD tests were performed using a Bruker-axs D5005HR diffractometer (Bruker-axs, Karlsruhe, Germany) equipped with a

two-crystal Ge (220) monochromator set for Cu-K $\alpha$ 1 radiation ( $\lambda = 1.54056 \text{ \AA}$ ). The accelerating voltage and tube current were 20 kV and 30 mA, and the step time and size were 0.1 s and  $0.001^\circ$ , respectively. The measured crystal wafers were (010) facet for  $\alpha$ -BIBO crystals and (001) facet for BZBO crystals, with both sides polished.

### 2.3. Characterization of Electro-Elastic Properties

The number of independent electro-elastic constants is relevant to the crystal symmetry. It is clear that the  $\alpha$ -BIBO belongs to the monoclinic symmetry with point group 2, while the BZBO crystal possesses orthorhombic symmetry with point group mm2. The related lattice parameters for  $\alpha$ -BIBO and BZBO crystals are presented in Table 1 [15,25]. Therefore, the electro-elastic constants of  $\alpha$ -BIBO and BZBO crystals are very different. The electro-elastic constants of these crystals were characterized by using the impedance method. The related crystal cuts, vibration modes, and equations for evaluating the independent dielectric, elastic, electromechanical, and piezoelectric constants were studied and reported in our previous work [18,21]. For the radial extensional mode, the effective electromechanical coupling factors  $k_p$  were evaluated by measuring the Y- and Z-oriented discs for  $\alpha$ -BIBO and BZBO crystals, respectively. The disc-shaped samples (6 pieces), with different dimension ratios, were prepared and vacuum-sputtered with platinum films (100–200 nm) on the two parallel faces. The capacitance, resonance and anti-resonance frequencies of the prepared samples were measured and recorded by using the multi-frequency LCR meter (Agilent 4263B) and impedance-phase gain analyzer HP4194A.

**Table 1.** Crystal lattice parameters for  $\alpha$ -BIBO and BZBO crystals [15,25].

Empirical Formula	$\alpha$ -BiB <sub>3</sub> O <sub>6</sub>	Bi <sub>2</sub> ZnB <sub>2</sub> O <sub>7</sub>
Formula weight	337.41	616.97
symmetry	monoclinic	orthorhombic
space group	C2	Pba2
a ( $\text{\AA}$ )	7.116 (2)	10.8268 (4)
b ( $\text{\AA}$ )	4.993 (2)	11.0329 (4)
c ( $\text{\AA}$ )	6.508 (3)	4.8848 (2)
V ( $\text{\AA}^3$ )	222.69	583.49 (19)
Z	2	4
density (Mg/m <sup>3</sup> )	5.033	7.036

## 3. Results and Discussion

### 3.1. Crystal Quality Evaluation

The crystal quality was assessed by using the HRXRD method. Figure 3 gives the rocking curves of the two oxyborate crystals, where the crystal samples for  $\alpha$ -BIBO and BZBO crystals were selected and prepared from the parts away from the seeding region. The diffraction peaks were symmetrical and the full-width at half-maximum values (FWHM) were obtained and found to be 35.35 arcsec and 47.85 arcsec for  $\alpha$ -BIBO and BZBO crystals, respectively. In order to characterize the homogeneity of the growth crystal, the HRXRD tests for different parts (away from the seeding region and close to the seeding region) of BZBO crystals were performed. The FWHM values for the crystal parts away from the seeding region were found smaller for both the  $\alpha$ -BIBO and BZBO crystals. The relative high FWHM value of the BZBO crystal sample prepared from the seeding region indicates that the initial growth process is vital for high quality crystal growth. It was also found that the crystal quality would improve as the crystal grows. In this study, the crystal samples were prepared from the good quality parts to get rid of the possible effects of crystal defects.

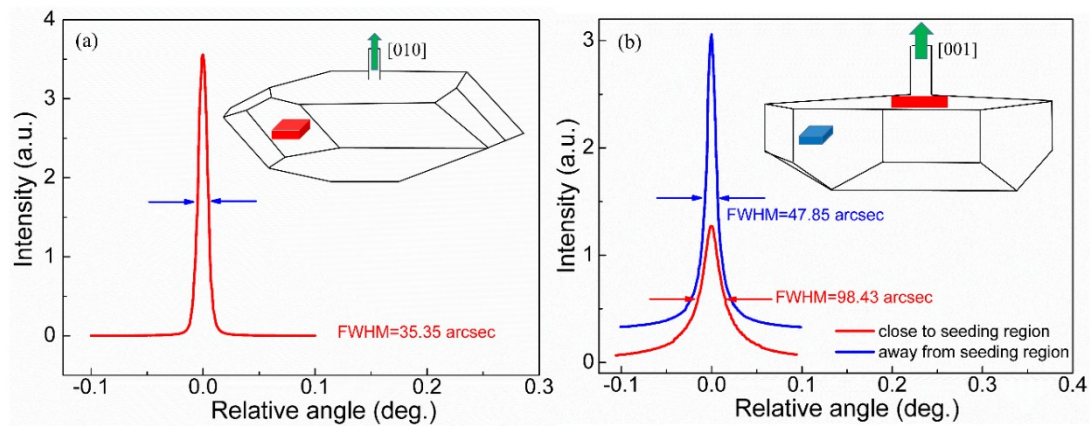


Figure 3. Rocking curves of the (010) wafers for  $\alpha$ -BIBO (a) and (001) wafers for BZBO (b).

### 3.2. Electro-Elastic Constants

The electro-elastic constants for  $\alpha$ -BIBO and BZBO crystals, measured at room temperature, are summarized in Table 2. Compared to the BZBO crystal, the  $\alpha$ -BIBO showed stronger piezoelectric response, where the longitudinal piezoelectric charge coefficient  $d_{22}$  was found to be 40 pC/N. In contrast, the BZBO crystal exhibited relatively weak piezoelectric properties, the largest piezoelectric charge coefficient was found for  $d_{32}$ , being  $-6.4$  pC/N, and the largest elastic compliance was obtained for  $s_{66}$ , being  $20.5$  pm<sup>2</sup>/N. The large piezoelectric activity of  $\alpha$ -BIBO crystal was presumed to be associated with the large structure distortions and net dipole moments. Figure 4 exhibits the schematic crystal structures for  $\alpha$ -BIBO and BZBO crystals, where the  $\alpha$ -BIBO crystal consists of one type of Bi-O octahedron, while the BZBO crystal possesses two types of Bi-O octahedra. Different from the  $\alpha$ -BIBO crystal, the directions of the dipole moment for the two types of Bi-O octahedra in BZBO crystal were partly offset, which weakened the piezoelectric response in BZBO crystal, thus the effective piezoelectric coefficients for BZBO crystal were lower than the  $\alpha$ -BIBO crystal [21,26,27].

Table 2. The electro-elastic constants of  $\alpha$ -BIBO and BZBO crystals measured at room temperature [18,21].

Elastic Compliances $s_{ij}^E$ (pm <sup>2</sup> ·N <sup>-1</sup> )													
	$s_{11}$	$s_{12}$	$s_{13}$	$s_{15}$	$s_{22}$	$s_{23}$	$s_{25}$	$s_{33}$	$s_{35}$	$s_{44}$	$s_{46}$	$s_{55}$	$s_{66}$
BIBO	36.2	-48.0	2.9	17.9	85.0	-2.6	-23.8	10.2	9.3	65.0	11.5	26.5	19.1
BZBO	8.2	-3.9	-1.5	\	11.8	-3.5	\	8.2	\	17.3	\	17.2	20.5
Elastic Stiffnesses $c_{ij}^E$ (10 <sup>10</sup> N·m <sup>-2</sup> )													
	$c_{11}$	$c_{12}$	$c_{13}$	$c_{15}$	$c_{22}$	$c_{23}$	$c_{25}$	$c_{33}$	$c_{35}$	$c_{44}$	$c_{46}$	$c_{55}$	$c_{66}$
BIBO	12.4	6.1	1.0	-3.2	4.7	-0.9	0.4	15.7	-7.0	1.7	-1.0	8.8	5.9
BZBO	17.0	7.4	6.3	\	13.1	6.9	\	16.4	\	5.8	\	5.8	4.9
Relative Dielectric Permittivities $\epsilon_{ij}^T/\epsilon_0$													
	$\epsilon_{11}$	$\epsilon_{13}$	$\epsilon_{22}$	$\epsilon_{33}$									
BIBO	12.0	-1.4	8.4	13.8									
BZBO	36.8	\	18.5	18.3									
Piezoelectric Charge Coefficients $d_{ij}$ (pC/N)													
	$d_{14}$	$d_{15}$	$d_{16}$	$d_{21}$	$d_{22}$	$d_{23}$	$d_{24}$	$d_{25}$	$d_{31}$	$d_{32}$	$d_{33}$	$d_{34}$	$d_{36}$
BIBO	10.9	\	13.9	16.7	40.0	2.5	\	4.3	\	\	\	18.7	13.0
BZBO	\	1.4	\	\	\	\	-5.5	\	2.5	-6.4	1.1	\	\
Electromechanical Coupling Factors $k_{ij}$ (%)													
	$k_{14}$	$k_{15}$	$k_{16}$	$k_{21}$	$k_{22}$	$k_{23}$	$k_{24}$	$k_{25}$	$k_{31}$	$k_{32}$	$k_{33}$	$k_{34}$	$k_{36}$
BIBO	13.1	\	30.9	32.1	50.0	9.2	\	9.6	\	\	\	21.0	26.9
BZBO	\	1.8	\	\	\	\	10.7	\	8.8	14.5	3.1	\	\

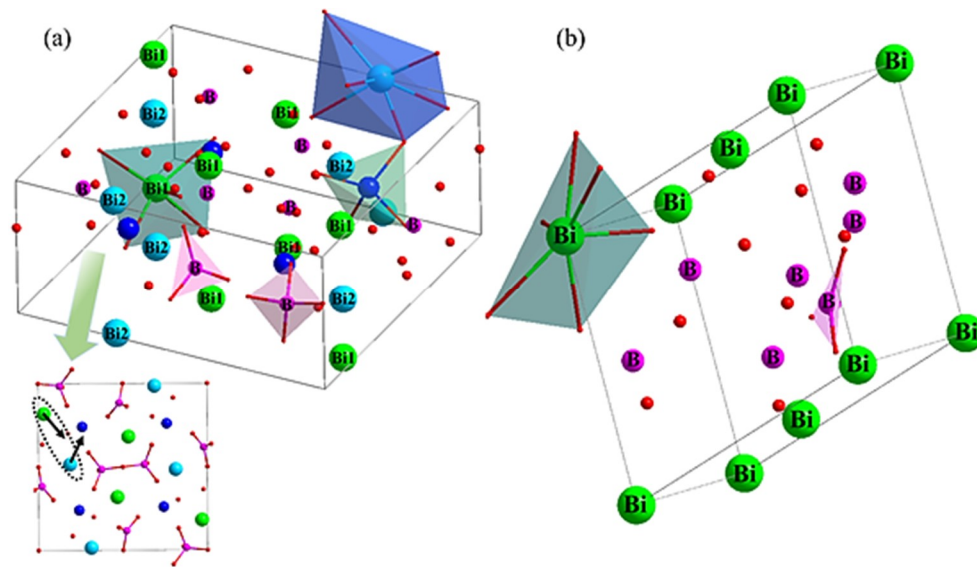


Figure 4. Crystal structures of BZBO (a) and  $\alpha$ -BIBO (b) crystals.

### 3.3. Characterization of Radial Extensional Vibration Mode

For the acoustic wave devices, there are many kinds of acoustic modes that can be utilized in a very wide frequency range (kHz~GHz). Among these acoustic waves, the lamb wave has been extensively studied [28–30]. The lamb wave can be excited using the radial extensional vibration mode. For the  $\alpha$ -BIBO and BZBO crystals, the electromechanical coupling factor  $k_p$ , relevant to the radial extensional vibration mode, was evaluated experimentally. The disc-shaped samples with different ratios were prepared for determining the  $k_p$  values. Using the empirical equation [31], as well as the measured resonant and anti-resonant frequencies, the radial extensional vibration mode electromechanical coupling factors  $k_p$ , for  $\alpha$ -BIBO and BZBO crystals, were obtained.

Figure 5 shows the obtained  $k_p$  values for the Y-oriented  $\alpha$ -BIBO and Z-oriented BZBO crystal discs. The small inset gives the recorded impedance-frequency spectra for the radial extensional vibration modes. It was observed that the difference of resonant and anti-resonant frequencies for the radial extensional mode of  $\alpha$ -BIBO was larger than that of BZBO crystal. The  $k_p$  values were determined to be in the order of 32.0% and 5.5% for the  $\alpha$ -BIBO and BZBO crystals, respectively.

### 3.4. Characterization of the Face Shear Vibration Mode

The face shear vibration mode could excite the guided wave along the crystal dimensional orientation, which could also be used for sensor application. According to the IEEE standard on piezoelectricity, there are three possible independent face shear mode piezoelectric coefficients in crystal, i.e.,  $d_{14}$ ,  $d_{25}$ , and  $d_{36}$ . In this work, the face shear vibration modes of  $\alpha$ -BIBO and BZBO crystals were discussed, taking advantage of the anisotropy of crystal materials. In order to design the optimum crystal cuts with large piezoelectric coefficients, the orientation dependences of the  $d_{14}$ ,  $d_{25}$ , and  $d_{36}$  corresponding to the XY, YZ, and ZX crystal cuts respectively were investigated (rotation angle around physical X-, Y-, and Z-axes was varied from  $-90^\circ$  to  $90^\circ$ ). Results are given in Figures 6 and 7.

For  $\alpha$ -BIBO single crystal, as shown in Figure 6, the shear mode piezoelectric coefficient  $d_{25}$  was found to be more sensitive to the rotation angle, compared with  $d_{14}$  and  $d_{36}$ . The variations of the  $d_{14}$  and  $d_{36}$ , rotated along the three physical axes, were symmetrically distributed, referring to the rotation angle at  $0^\circ$ . The piezoelectric coefficient  $d_{25}$  changed from  $-13$  pC/N to  $4.3$  pC/N, and from  $-10.9$  pC/N to  $4.3$  pC/N, as the angle rotated around the X- and Z-axes, respectively. In contrast, the largest piezoelectric coefficient  $d_{25}$  (YZ cut) was obtained and found to be in the order of  $14.8$  pC/N and  $-14.8$  pC/N, when the rotation angle reached at  $37^\circ$  and  $-53^\circ$  around the Y-axis (the small inset of Figure 6), respectively, more than two times that of langasite crystal ( $d_{14} = -6.01$  pC/N) [32].

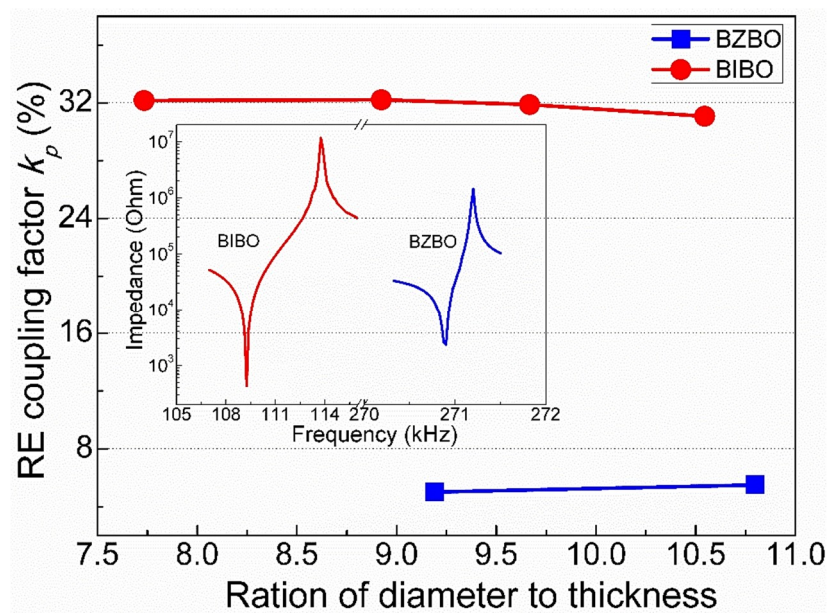


Figure 5. The radial extensional electromechanical coupling factor  $k_p$  for the  $\alpha$ -BIBO and BZBO crystals.

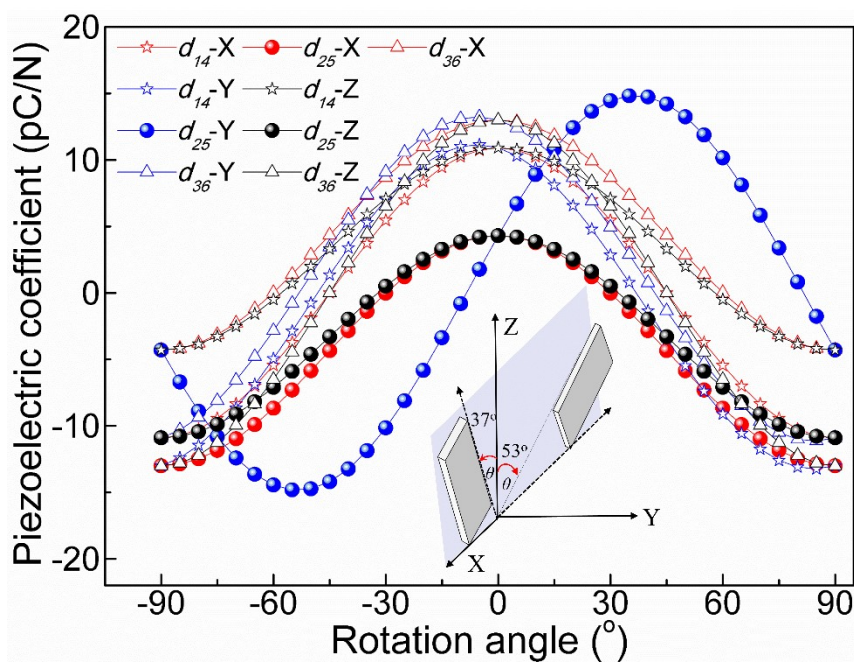
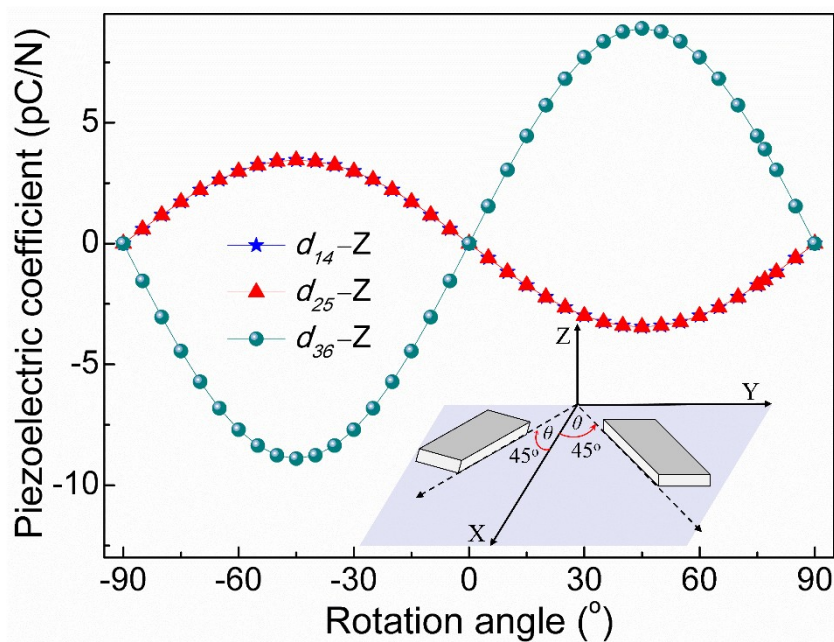


Figure 6. Orientation dependence of piezoelectric coefficient rotated around X-, Y- and Z-axes for  $\alpha$ -BIBO crystals. The small inset shows the crystal cuts ( $YZt/37^\circ$  and  $YZt/-53^\circ$ ) with largest  $d_{25}$  value.

The face shear mode piezoelectric coefficients  $d_{14}$ ,  $d_{25}$  and  $d_{36}$  for BZBO crystal are also studied and the results are given in Figure 7. The BZBO crystal was found to show very limited face shear modes, due to the crystal symmetry. The effective face shear mode piezoelectric coefficients  $d_{14}$ ,  $d_{25}$  and  $d_{36}$  were only observed when rotated around the physical Z-axis. The effective piezoelectric coefficient  $d_{14}$  equaled to the  $d_{25}$ , as a function of rotation angle around the Z-axis. The largest values were found to be  $\pm 3.5$  pC/N when the rotation angles reached  $\pm 45^\circ$ . Differently, the piezoelectric coefficient  $d_{36}$  varied from  $-8.9$  pC/N to  $8.9$  pC/N, when the rotation angle shifted from  $-90^\circ$  to  $90^\circ$ . The maximum value of  $d_{36}$  (ZX crystal cut) was determined to be in the order of  $\pm 8.9$  pC/N when the rotation angle approached to  $\pm 45^\circ$ . Thus, the optimal face shear mode piezoelectric crystal cuts were found to be  $(ZXt)/\pm 45^\circ$  for BZBO crystal, as presented in the small inset of Figure 7.



**Figure 7.** Orientation dependences of piezoelectric coefficient rotated around Z-axis for BZBO crystals. The small inset shows the optimum crystal cuts ( $(ZXt)/\pm 45^\circ$  crystal cuts) with the largest  $d_{36}$ .

#### 4. Conclusions

In this study, single crystal growth of bismuth-based oxyborate crystals  $\alpha$ -BIBO and BZBO was introduced. The quality of the  $\alpha$ -BIBO and BZBO crystals grown by the Kyropoulos method was assessed using the HRXRD method. The results indicate that the crystals part away from the seeding region exhibiting high crystal quality. The electro-elastic properties of  $\alpha$ -BIBO and BZBO crystals were evaluated at room temperature taking advantage of the impedance method, where the  $\alpha$ -BIBO crystal showed stronger piezoelectric response than the BZBO crystal. In addition, the radial extensional and face shear vibration modes were studied. The radial extensional electromechanical coupling factors  $k_p$  were evaluated to be 32.0% and 5.5% for  $\alpha$ -BIBO and BZBO crystals, respectively. Furthermore, the optimal face shear mode crystal cuts were obtained and found to be  $(YZt)/-53^\circ$  and  $(YZt)/37^\circ$  for  $\alpha$ -BIBO crystal, and  $(ZXt)/\pm 45^\circ$  cuts for BZBO crystal. These crystal cuts are a potential for acoustic wave device application.

**Author Contributions:** Conceptualization, F.C. and F.Y.; Investigation, F.C.; Methodology, F.C., X.C., F.Y. and C.W.; Resources, F.Y. and X.Z.; Validation, F.Y. and X.Z.; Writing—original draft, F.C.; Writing—review and editing, F.Y.

**Funding:** This research was financially supported by the Primary Research and Development Plan of Shandong Province (2017CXGC0413) and the National Nature Science Foundation of China (51872165).

**Acknowledgments:** The authors would like to thank Fangming Zuo at Jinan SCK photonics Co., Ltd. for sample preparation.

**Conflicts of Interest:** The authors declare no conflicts of interest.

#### References

1. Yang, Y.; Jiang, X.X.; Lin, Z.S.; Wu, Y.C. Borate-based ultraviolet and deep-ultraviolet nonlinear optical crystals. *Crystals* **2017**, *7*, 95. [[CrossRef](#)]
2. Bubnova, R.; Volkov, S.; Albert, B.; Filatov, S. Borates-crystal structures of prospective nonlinear optical materials: High anisotropy of the thermal expansion caused by anharmonic atomic vibrations. *Crystals* **2017**, *7*, 93. [[CrossRef](#)]
3. Wu, Y.C.; Sasaki, T.; Nakai, S.; Yokotani, A.; Tang, H.G.; Chen, C.T.  $\text{CsB}_3\text{O}_5$ : A new nonlinear optical crystal. *Appl. Phys. Lett.* **1993**, *62*, 2614–2615. [[CrossRef](#)]

4. Aka, G.; Kahn-Harari, F.; Mougél, F.; Vivien, D. Linear- and nonlinear-optical properties of a new gadolinium calcium oxoborate crystal,  $\text{Ca}_4\text{GdO}(\text{BO}_3)_3$ . *J. Opt. Soc. Am. B* **1997**, *14*, 2238–2247. [[CrossRef](#)]
5. Sasaki, T.; Mori, Y.; Yoshimura, M.; Yap, Y.K.; Kamimura, T. Recent development of nonlinear optical borate crystals: Key materials for generation of visible and UV light. *Mater. Sci. Eng.* **2000**, *30*, 1–54. [[CrossRef](#)]
6. Mori, Y.; Yap, Y.K.; Kamimura, T.; Yoshimura, M.; Sasaki, T. Recent development of nonlinear optical borate crystals for UV generation. *Opt. Mater.* **2002**, *19*, 1–5. [[CrossRef](#)]
7. Hu, C.; Mutailipu, M.; Wang, Y.; Guo, F.J.; Yang, Z.H.; Pan, S.L. The activity of lone pair contributing to SHG response in bismuth borates: A combination investigation from experiment and DFT calculation. *Phys. Chem. Chem. Phys.* **2017**, *19*, 25270–25276. [[CrossRef](#)]
8. Lin, Z.S.; Wang, Z.Z.; Chen, C.T.; Lee, M.H. Mechanism for linear and nonlinear optical effects in monoclinic bismuth borate ( $\text{BiB}_3\text{O}_6$ ) crystal. *J. Appl. Phys.* **2001**, *90*, 5585–5590. [[CrossRef](#)]
9. Levin, E.M.; Mcdaniel, C.L. The System  $\text{Bi}_2\text{O}_3$ - $\text{B}_2\text{O}_3$ . *J. Am. Ceram. Soc.* **1962**, *45*, 355–360. [[CrossRef](#)]
10. Burianer, M.; Mvhlberg, M. Crystal growth of boron sillenite  $\text{Bi}_{24}\text{B}_2\text{O}_{39}$ . *Cryst. Res. Technol.* **1997**, *32*, 1023–1027. [[CrossRef](#)]
11. Filatov, S.; Shepelev, Y.; Bubnova, R.; Sennova, N.; Egorysheva, A.V.; Kargin, Y.F. The study of  $\text{Bi}_3\text{B}_5\text{O}_{12}$ : Synthesis, crystal structure and thermal expansion of oxoborate  $\text{Bi}_3\text{B}_5\text{O}_{12}$ . *J. Solid State Chem.* **2004**, *177*, 515–522. [[CrossRef](#)]
12. Becker, P.; Liebertz, J.; Bohatý, L. Top-seeded growth of bismuth triborate,  $\text{BiB}_3\text{O}_6$ . *J. Cryst. Growth* **1999**, *203*, 149–155. [[CrossRef](#)]
13. Zhang, K.C.; Chen, X.A.; Wang, X.M. Review of study on bismuth triborate ( $\text{BiB}_3\text{O}_6$ ) crystal. *J. Synth. Cryst.* **2005**, *34*, 438–443.
14. Wang, Z.P.; Teng, B.; Fu, K.; Xu, X.G.; Song, R.B.; Du, C.L.; Jiang, H.D.; Wang, J.Y.; Liu, Y.G.; Shao, Z.S. Efficient second harmonic generation of pulsed laser radiation in  $\text{BiB}_3\text{O}_6$  (BIBO) crystal with different phase matching directions. *Opt. Commun.* **2002**, *202*, 217–220. [[CrossRef](#)]
15. Barbier, J.; Penin, N.; Cranswick, L.M. Melilite-type borates  $\text{Bi}_2\text{ZnB}_2\text{O}_7$  and  $\text{CaBiGaB}_2\text{O}_7$ . *Chem. Mater.* **2005**, *17*, 3130–3136. [[CrossRef](#)]
16. Li, F.; Pan, S.L.; Hou, X.L.; Yao, J. A novel nonlinear optical crystal  $\text{Bi}_2\text{ZnOB}_2\text{O}_6$ . *Cryst. Growth Des.* **2009**, *9*, 4091–4095. [[CrossRef](#)]
17. Teng, B.; Wang, J.Y.; Wang, Z.P.; Hu, X.B.; Jiang, H.D.; Liu, H.; Cheng, X.F.; Dong, S.M.; Liu, Y.G.; Shao, Z.S. Crystal growth, thermal and optical performance of  $\text{BiB}_3\text{O}_6$ . *J. Cryst. Growth* **2001**, *233*, 282–286. [[CrossRef](#)]
18. Yu, F.P.; Lu, Q.M.; Zhang, S.J.; Wang, H.W.; Cheng, X.F.; Zhao, X. High-performance, high-temperature piezoelectric  $\text{BiB}_3\text{O}_6$  crystals. *J. Mater. Chem. C* **2015**, *3*, 329–338. [[CrossRef](#)]
19. Li, F.; Hou, X.L.; Pan, S.L.; Wang, X. Growth, structure, and optical properties of a congruent melting oxyborate,  $\text{Bi}_2\text{ZnOB}_2\text{O}_6$ . *Chem. Mater.* **2009**, *21*, 2846–2850. [[CrossRef](#)]
20. Chen, F.F.; Wang, X.L.; Wei, L.; Yu, F.P.; Tian, S.W.; Jiang, C.; Li, Y.L.; Cheng, X.F.; Wang, Z.P.; Zhao, X. Thermal properties and CW laser performances of pure and Nd doped  $\text{Bi}_2\text{ZnB}_2\text{O}_7$  single crystals. *CrystEngComm* **2018**, *20*, 7094–7099. [[CrossRef](#)]
21. Chen, F.F.; Jiang, C.; Tian, S.W.; Yu, F.P.; Cheng, X.F.; Duan, X.L.; Wang, Z.P.; Zhao, X. Electroelastic features of piezoelectric  $\text{Bi}_2\text{ZnB}_2\text{O}_7$  crystal. *Cryst. Growth Des.* **2018**, *18*, 3988–3996. [[CrossRef](#)]
22. Kauffmann, P.; Ploix, M.A.; Chaix, J.F.; Gueudré, C.; Corneloup, G.; Baqué, F. Study of lamb waves for non-destructive testing behind screens. *EPJ Web Conf.* **2018**, *170*, 1–3. [[CrossRef](#)]
23. Rguiti, M.; Grondel, S.; El youbi, F.; Courtois, C.; Lippert, M.; Leriche, A. Optimized piezoelectric sensor for a specific application: Detection of lamb waves. *Sens. Actuators A* **2006**, *126*, 362–368. [[CrossRef](#)]
24. Giurgiutiu, V. *Structural Health Monitoring, with Piezoelectric Wafer Active Sensors*; Elsevier: Amsterdam, The Netherlands, 2007.
25. Fröhlich, V.R.; Bohatý, U.L.; Lieberta, J. Die kristallstruktur von wismutborat,  $\text{BiB}_3\text{O}_6$ . *Acta Cryst.* **1984**, *C40*, 343–344. [[CrossRef](#)]
26. Brese, N.E.; Keeffe, M.O. Bond-valence parameters for solids. *Acta Cryst.* **1991**, *B47*, 192–197. [[CrossRef](#)]
27. Maggard, P.A.; Nault, T.S.; Stern, C.L.; Kenneth, R.P. Alignment of acentric  $\text{MoO}_3\text{F}_3^{3-}$  anions in a polar material:  $(\text{Ag}_3\text{MoO}_3\text{F}_3)(\text{Ag}_3\text{MoO}_4)\text{Cl}$ . *J. Solid State Chem.* **2003**, *175*, 27–33. [[CrossRef](#)]
28. Su, Z.Q.; Ye, L.; Lu, Y. Guided lamb waves for identification of damage in composite structures: A review. *J. Sound Vib.* **2006**, *295*, 753–780. [[CrossRef](#)]

29. Kuypers, J.H.; Pisano, A.P. Interpolation technique for fast analysis of surface acoustic wave and lamb wave devices. *Jpn. J. Appl. Phys.* **2009**, *48*, 07GG07. [[CrossRef](#)]
30. Schmitt, M.; Olfert, S.; Rautenberg, J.; Lindner, G.; Henning, B.; Reindl, L.M. Multi reflection of lamb wave emission in an acoustic waveguide sensor. *Sensors* **2013**, *13*, 2777–2785. [[CrossRef](#)]
31. Li, Y.; Qin, Z.K. *Measurement of Piezoelectric and Ferroelectric Materials*; Science Press: Beijing, China, 1984.
32. Bohm, J.; Chilla, E.; Flannery, C.; Frohlich, H.J.; Hauke, T.; Heimann, R.B.; Hengst, M.; Straube, U. Czochralski growth and characterization of piezoelectric single crystals with langasite structure:  $\text{La}_3\text{Ga}_5\text{SiO}_{14}$  (LGS),  $\text{La}_3\text{Ga}_{5.5}\text{Nb}_{0.5}\text{O}_{14}$  (LGN) and  $\text{La}_3\text{Ga}_{5.5}\text{Ta}_{0.5}\text{O}_{14}$  (LGT) II. Piezoelectric and elastic properties. *J. Cryst. Growth* **2000**, *216*, 293–298. [[CrossRef](#)]



© 2019 by the authors. Licensee MDPI, Basel, Switzerland. This article is an open access article distributed under the terms and conditions of the Creative Commons Attribution (CC BY) license (<http://creativecommons.org/licenses/by/4.0/>).